RSC Advances

This is an *Accepted Manuscript*, which has been through the Royal Society of Chemistry peer review process and has been accepted for publication.

Accepted Manuscripts are published online shortly after acceptance, before technical editing, formatting and proof reading. Using this free service, authors can make their results available to the community, in citable form, before we publish the edited article. This *Accepted Manuscript* will be replaced by the edited, formatted and paginated article as soon as this is available.

You can find more information about *Accepted Manuscripts* in the Information for Authors.

Please note that technical editing may introduce minor changes to the text and/or graphics, which may alter content. The journal's standard Terms & Conditions and the Ethical guidelines still apply. In no event shall the Royal Society of Chemistry be held responsible for any errors or omissions in this *Accepted Manuscript* or any consequences arising from the use of any information it contains.

ROYAL SOCIETY OF CHEMISTRY

www.rsc.org/advances

Effect of acrylonitrile content on compatibility and damping properties of hindered phenol AO-60/nitrile-butadiene rubber composites: Molecular dynamics simulation

Meng Song,[a] Xiuying Zhao,[a,b] Yi Li,[a] Tung W. Chan,[c] Liqun Zhang[a,b] and Sizhu Wu[a*]

[a]Beijing Engineering Research Center of Advanced Elastomers, Beijing University of Chemical Technology, Beijing 100029, P.R. China

[b]Engineering Research Center of Elastomer Materials Energy Conservation and Resources，Ministry of Education, Beijing University of Chemical Technology, Beijing 100029, P.R. China

[c]Department of Materials Science and Engineering, Virginia Polytechnic Institute and State University, Blacksburg, VA 24061, USA

Corresponding author: Sizhu Wu (E-mail: wusz@mail.buct.edu.cn)

The effect of the acrylonitrile content in NBR on the compatibility and damping properties of AO-60/NBR was investigated by molecular dynamics (MD) simulation and experimental methods. The hindered phenol AO-60 had poor compatibility with nitrile-butadiene rubber (NBR) with an acrylonitrile content of 41% (denoted by N220S), but had good compatibility with NBR with an acrylonitrile content of 34% (denoted by N230S). The AO-60/N230S composite had larger H-bonds and higher binding energy than the AO-60/N220S composite at the same AO-60 content, both indicating stronger interactions between N230S and AO-60 and better damping

RSC Advances Accepted Manuscript

performance of AO-60/N230S. Moreover, SEM, DSC, and DMA were used to evaluate the compatibility and damping of AO-60/NBR composites. Phase separation occurred between N220S and AO-60, but a fine dispersion of AO-60 in N230S was obtained. The present study hopes to provide theoretical guidance to the design damping rubber materials.

1 Introduction

Rubber damping materials, the fastest growing polymer systems, have found increasing applications in all kinds of motor vehicles, instruments, automatic office facilities, household appliances, and aerospace engineering.[1, 2] Rubber damping materials offer a variety of advantages over conventional damping materials in minimizing mechanical noises, reducing mechanical vibrations, enhancing work efficiency, and improving product quality.[3, 4] In recent years, the invention of rubber damping materials has led to further interest in organic hybrids with high damping properties. [5-7] Organic hybrids are based on the hydrogen bonds (H-bonds) formed between small organic molecules and rubber matrixes.[8-10]

Previous studies showed that the introduction of the hindered phenol tetrakis [methylene-3-(3-5-ditert-butyl-4-hydroxy phenyl)propionyloxy]methane (AO-60) into nitrile-butadiene rubber (NBR) matrixes can form a composite with better damping properties than those of the rubber mattrix.[11-13] Compatibility is the key factor in choosing organic hybrid components and determining structure and performance.[14, 15] Because of the -CN side groups, NBR has strong polarity and high loss factor.[16, 17]

RSC Advances Accepted Manuscript

The acrylonitrile content in NBR will affect the compatibility of small organic molecules and NBR, and the damping properties of the composite.[18, 19]

A number of experiments, including optical microscopy,[20] neutron scattering,[21] differential scanning calorimetry (DSC),[22] inverse gas chromatography,[23] and dynamic mechanical analysis (DMA)[24] were conducted in the past to investigate the compatibility. However, the compatibility can also be characterized by molecular dynamics (MD) simulation.[25] With the development of powerful computer hardware and software, MD simulation proves to be a promising tool for material development and design because it can reveal molecular mechanisms that are hard to obtain by experimental methods. [26, 27]

To the best of our knowledge, there has not been a study that critically examines the compatibility, structure, and damping properties of AO-60/NBR composites with different acrylonitrile contents by a combined experimental and MD simulation method. It was consequently our goal to carry out such a study.

2 Simulation and Results

2.1 MD simulation strategies

The MD simulations were carried out by using the DISCOVER and AMORPHOUS CELL modules from Accelrys (San Diego, CA) with the Condensed-Phase Optimized Molecular Potentials for Atomistic Simulation Studies (COMPASS) force field.[28] In this force field, the total potential energy (E_{pot}) is expressed as

$$E_{pot} = E_b + E_\theta + E_\phi + E_\chi + E_{cross} + E_{Cou} + E_{vdW} \quad (1)$$

RSC Advances Accepted Manuscript

where E_b is the bond stretching energy, E_θ is the angle bending energy, E_Φ is the dihedral torsion energy, E_χ is the out-of-plane energy, E_{cross} is the cross-term interaction energy, E_{Cou} is the Coulombic interaction energy, and E_{vdW} is the van der Waals interaction energy. The first five terms represent the short-range bonded interactions, whereas the last two terms represent the inter- and intra-molecular non-bonded interactions.[29] Fig. 1 shows the acrylonitrile repeating unit, butadiene repeating unit, and NBR polymer chains at different acrylonitrile contents. After the atomistic repeating units of acrylonitrile and butadiene were prepared (see Fig.1 (a) and (b)), single random copolymer chains (NBR) with the mass fractions of acrylonitrile of 41% (Fig.1 (c), denoted by N220S polymer chain) and 34% (Fig.1 (d), denoted by N230S polymer chain), each with 30 repeating units, were constructed.

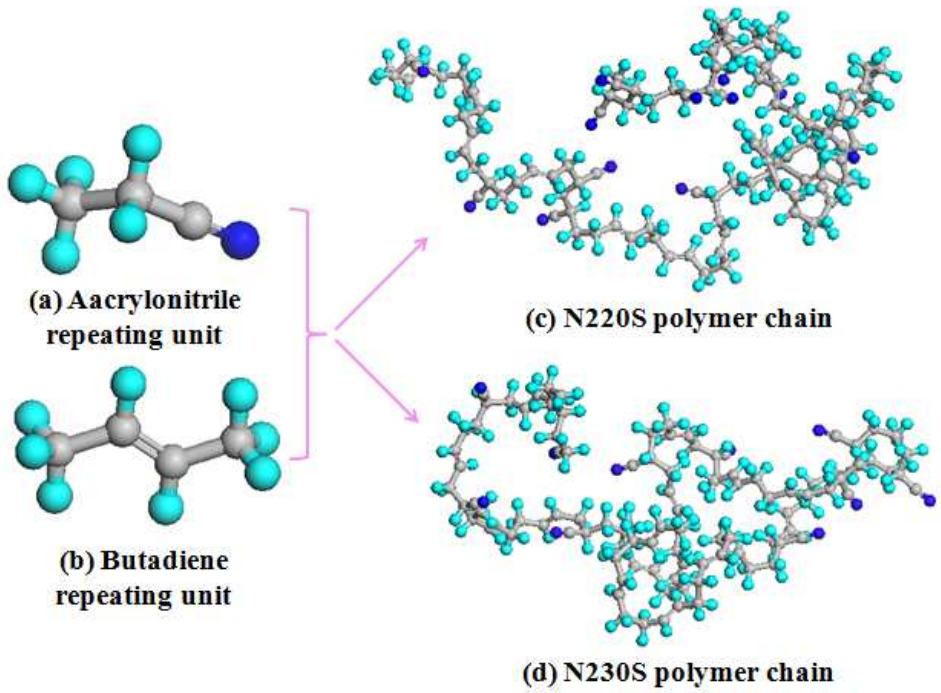

Fig.1 (a) Acrylonitrile repeating unit, (b) butadiene repeating unit, (c) N220S polymer chain, and (d) N230S polymer chain in MD simulation (grey, cyan and blue spheres stand for C, H, and N atoms, respectively).

RSC Advances Accepted Manuscript

Fig. 2 shows the process of construction of the amorphous cell. First, the NBR polymer chains (Fig.2 (a)) and AO-60 small molecules (Fig.2 (b)) are built in a periodic boundary cell (Fig.2 (c)). Amorphous cells containing composites of N220S polymer chains and AO-60 small molecules (or N230S polymer chains with AO-60 small molecules) are constructed, and periodic boundary conditions are applied. There are four N220S (or N230S) polymer chains and some AO-60 small molecules in each cell with mass ratios of AO-60 to NBR of 0/100, 36/100, and 73/100. Then the energy of each generated cell is minimized to a convergence value of 1.0×10^{-5} kcal/mol/Å by using the Smart Minimizer method to relax the state of minimal potential energy. The cell is then annealed at 0.1 MPa from the lower temperature of 200 K to the upper temperature of 400 K for 50 ps to prevent the system to form being trapped at a local high energy minimum.[30] Subsequently, 150 ps of NVT (constant number of particles, volume, and temperature) simulation is performed at 298 K and 200 ps of NPT (constant number of particles, pressure, and temperature) simulation is performed at 0.1 MPa to further relax the polymer structure by using the Andersen Thermostat[31] for temperature control and the Berendsen Barostat for pressure control[32] (Fig.2 (d)). At last, the cell can be used to analyze the properties of the system.

RSC Advances Accepted Manuscript

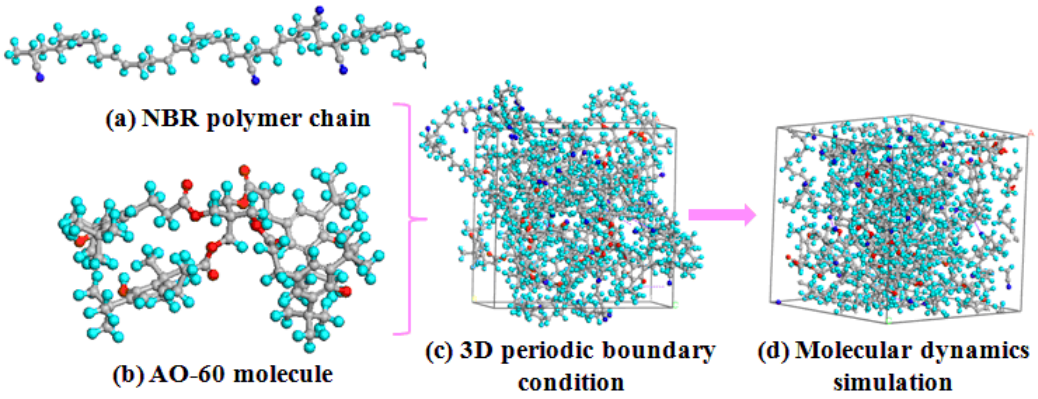

Fig. 2 Models for MD simulation of AO-60/NBR composite (blue sphere is N, red sphere is O, cyan sphere is H, and grey sphere is C)

2.2 Analysis of AO-60/NBR composites by MD simulation

In MD simulation, there are two equilibrium criteria: one is the equilibrium of temperature, and the other is the equilibrium of energy. The equilibration time depends on the number of atoms in a specific system.[33, 34] When the fluctuations of temperature and energy are in the range of 5 to 10%, the equilibrium of the system is reached. Our MD systems have reached equilibrium, as shown in Figs. 3 and 4.

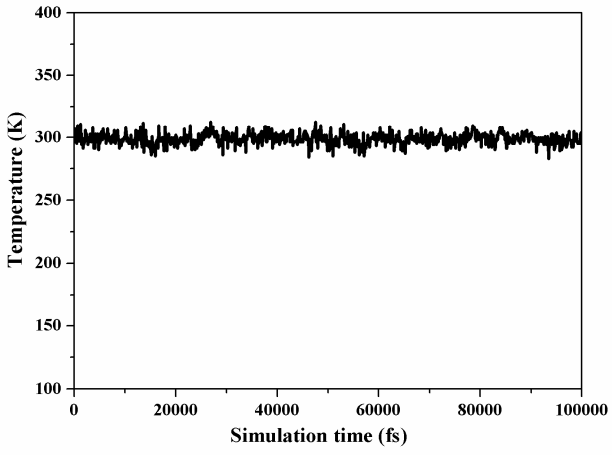

Fig. 3 Temperature vs. simulation time

RSC Advances Accepted Manuscript

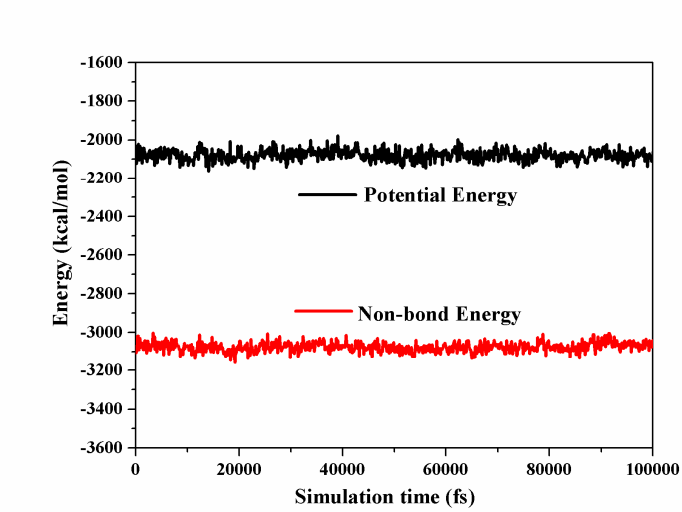

Fig. 4 Energy vs. simulation time

The packing modes and structures of polymers are very sensitive to small variations on cell densities.[35] The MD simulation density values are summarized in Table 1 and are in reasonably good agreement with the experimental results ($|\rho_{MD}-\rho_{Exp}| < 0.1$), although the presence of a few additives in the experimental samples are not account for in the MD simulation. [36]

Table 1 MD simulation and experimental density of AO-60/NBR composites

Compounds	Experimental density (g/cm^3)	Simulated density (g/cm^3)
AO-60/N220S (0/100)	1.059	1.030
AO-60/N220S (36/100)	1.068	1.041
AO-60/N220S (73/100)	1.028	0.9407
AO-60/N230S (0/100)	1.032	0.9545
AO-60/N230S (36/100)	1.044	1.018
AO-60/N230S (73/100)	1.050	1.024

The solubility parameter (δ) characterizes the strength of the cohesion between polymer molecules; thus, it is an important parameter to evaluate the compatibility of polymer blends.[37] The solubility parameter δ is defined as the square root of the

RSC Advances Accepted Manuscript

cohesive energy density (CED):

$$\delta = (CED)^{\frac{1}{2}} = \left(\frac{\Delta E}{V}\right)^{\frac{1}{2}} = \left(\frac{\Delta H_v - RT}{V}\right)^{\frac{1}{2}} \quad (2)$$

where $\triangle E$ is the change in internal energy of vaporization, $\triangle H$ is enthalpy of vaporization, V is the molar volume, R is the gas constant, and T is the absolute temperature. Empirically, if the difference δ_A-δ_B between the two components A and B is less than 1.0 $(cal/cm^3)^{1/2}$, the two components are compatible.[38] If δ_A-δ_B is larger than 1.0 $(cal/cm^3)^{1/2}$ and less than 3.4 $(cal/cm^3)^{1/2}$, A and B are probably compatible. However, if δ_A-δ_B is larger than 4.9 $(cal/cm^3)^{1/2}$, A and B are incompatible.[39] The simulated solubility parameter differences between N220S or N230S and AO-60 computed are summarized in Table 2.

Table 2 Predictions of compatibility for AO-60/NBR from MD simulation

Components	Solubility parameters (δ_{MD}) $(cal/cm^3)^{1/2}$	δ_{NBR}-$\delta_{AO\text{-}60}$ $(cal/cm^3)^{1/2}$	Interpretation
N220S	9.45	1.24	likely to compatible
N230S	9.07	0.86	compatible
AO-60	8.21	----	----

As seen in Table 2, it is evident from the data that AO-60/N230S has good compatibility owing to the small $\Delta\delta$ (δ_{N230S}-$\delta_{AO\text{-}60}$ < 1.0) between the two components. However, the greater $\Delta\delta$ between N220S and AO-60 indicatives that N220S and AO-60 are likely to be compatible. These predictions were confirmed by DSC and DMA experiments, as described in the next section.

The compatibility between NBR and AO-60 is attributed to H-bonds formation. MD simulation can obtain quantitative information on the H-bonds in AO-60/NBR composites. Fig.5 shows the simulated hydrogen bonds in an amorphous cell for the

RSC Advances Accepted Manuscript

AO-60/N230S (73/100) composite. There are two kinds of H-bonds in the AO-60/NBR composite. The first H-bond$_{(a)}$ O-H···O is between the phenolic hydroxyl groups –OH of AO-60 and the carbonyl groups –C=O of AO-60. The second, H-bond$_{(b)}$ O-H···N, is between the phenolic hydroxyl groups –OH of AO-60 and the nitrile groups –CN of NBR.

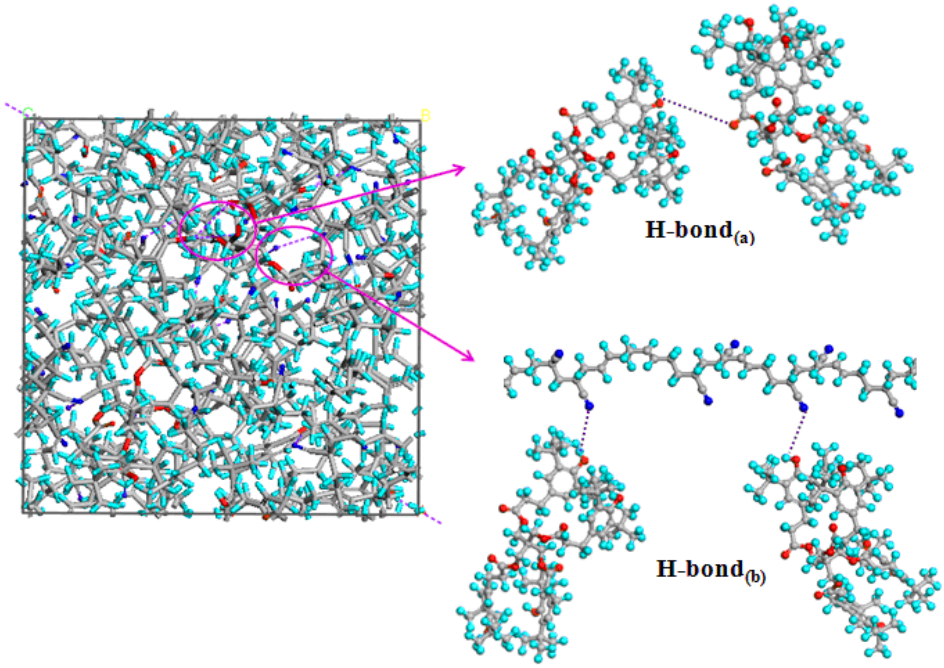

Fig.5 H-bonds in amorphous cell of AO-60/N230S (73/100) (the purple dotted lines represent H-bonds)

Through repeated simulations, the number of H-bonds in AO-60/NBR composites with different mass ratios were obtained and listed in Table 3.

Table 3 Number of H-bonds$_{(a)}$ and H-bonds$_{(b)}$ in different AO-60/NBR composites.

Composites	AO-60/N220S (36/100)	AO-60/N220S (73/100)	AO-60/N230S (36/100)	AO-60/N230S (73/100)
No. of H-bonds$_{(a)}$	2	1	4	3
No. of H-bonds$_{(b)}$	5	3	6	6

There is no H-bond in the N220S or N230S matrix. The addition of AO-60

RSC Advances Accepted Manuscript

molecules leads to the formation of H-bonds in the AO-60/N220S (or AO-60/N230S) composite. The number of H-bonds in AO-60/N230S is larger than that in AO-60/N220S at the same AO-60 content, indicating the stronger interaction between AO-60 and N230S and the better damping property of AO-60/N230S.

The binding energy ($E_{binding}$) which is defined as the negative value of the interaction energy (E_{inter}), can well reflect the intermolecular interactions and the mixing capacity of two components.[33, 36] The binding energy is calculated by the follow equation:

$$E_{binding} = -E_{inter} = -\left(E_{total} - E_{AO\text{-}60} - E_{NBR}\right) \quad (3)$$

where E_{total} is the total energy of the system, $E_{AO\text{-}60}$ is the energy of AO-60, and E_{NBR} is the energy of NBR. E_{N220S} and E_{N230S} are constant (-1227.489 kcal/mol and -1034.816 kcal/mol, respectively) because in the MD simulation we fix the number of N220S and N230S chains in the cell. All the energies can be obtained from the equilibrium configuration of trajectory files at the end of a MD simulation.

Table 4 presents the binding energy of N220S, N230S, the AO-60/N220S composite, and the AO-60/N230S composite. N230S has a stronger capability to blend with AO-60 molecules than N220S due to the larger number of H-bonds formed, indicating the stronger interaction and better compatibility between N230S and AO-60. The binding energy of the AO-60/N220S composite is negative when the AO-60 content exceeds 36 phr, indicating the incompatibility of the N220S matrix and AO-60 molecules, and phase separation will occur in the AO-60/N220S composite. These results are consistent with the above predictions based on the solubility parameter δ.

RSC Advances Accepted Manuscript

Table 4 Binding energies of N220S, N230S, AO-60/N220S, and AO-60/N230S.

Composites	Mass ratios	E_{total} (kcal/mol)	E_{AO-60} (kcal/mol)	$E_{binding}$ (kcal/mol)
AO-60/N220S	36/100	-1753.360	-430.989	116.496
	73/100	-2114.470	-972.170	-63.575
AO-60/N230S	36/100	-1606.29	-447.336	124.142
	73/100	-2072.783	-1014.724	23.243

Thus, by MD simulation, the solubility parameter, H-bonds, and binding energy of the AO-60/NBR composites are calculated. AO-60/N230S has smaller solubility parameter difference between the components than AO-60/N220S., indicating a good compatibility between N230S and AO-60. Moreover, AO-60/N230S has larger H-bonds and higher binding energy than AO-60/N220S, indicating good damping performance of AO-60/N230S and. These theoretical predictions will be confirmed by experiments below.

3 Experiments and Comparison with Theoretical Results

3.1 Materials

NBR (N220S) with an acrylonitrile mass fraction of 41% and NBR (N230S) with an acrylonitrile mass fraction of 34% were provided by Japan Synthetic Rubber Co., Ltd. (Tokyo, Japan). AO-60 in the form of powder was purchased from Beijing Additives Institute (Beijing, China). The chemical structure of AO-60 is shown in Fig. 6. Other chemicals and ingredients were all purchased in China. All materials were used without further purification.

RSC Advances Accepted Manuscript

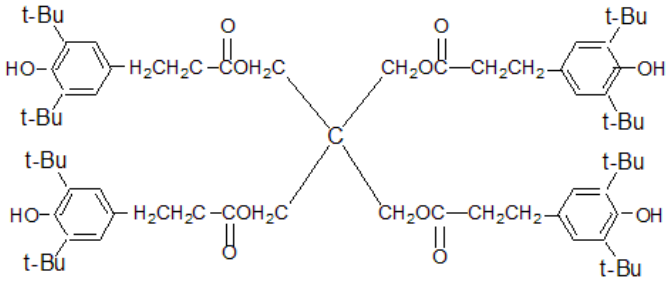

Fig. 6 Molecular structure of AO-60

3.2 Sample preparation

AO-60/NBR rubber composites were prepared according to the following procedures: (1) After the as-received NBR was kneaded on a Φ152.4 mm two-roll mill at room temperature for 3 min, AO-60 was blended in the AO-60/NBR mass ratios of 0/100, 36/100, and 73/100 into equal amounts of the kneaded NBR by kneading at room temperature for 5 min to form the first-stage AO-60/NBRa composites. (2) Each AO-60/NBRa composite was kneaded on the two-roll mill at 130℃ for 5 min to fully fuse the AO-60 small molecules before the composite was gradually cooled to room temperature to form a second-stage AO-60/NBRb composite. (3) The AO-60/NBRb composite was then blended with compounding and crosslinking additives, including 5.0 phr of zinc oxide, 2.0 phr of stearic acid, 0.5 phr of dibenzothiazole disulfide, 0.5 phr of diphenyl guanidine, 0.2 phr of tetramethylthiuram disulfide, and 2.0 phr of sulfur by kneading on the two-roll mill at room temperature for 10 min. (4) Finally, the composite was vulcanized on a hot press at 160℃ under the pressure of 15 MPa for the optimum vulcanization time to form an AO-60/NBR sample. The optimum vulcanization time was pre-determined for each composite by using a disc rheometer (P355C2) manufactured by Huanfeng Chemical

RSC Advances Accepted Manuscript

Technology and Experimental Machine Co. (Beijing, China).

3.3 Characterization

SEM images were taken of representative fracture surfaces of the AO-60/NBR composites by using a Hitachi S-4800 high resolution SEM (Japan). The SEM specimens were prepared by fracturing the composites in liquid nitrogen. FTIR measurements were made with a Nicolet 8700 FTIR spectrometer made by Thermo Fisher Scientific Inc. (USA). The FTIR spectra were obtained by scanning the specimens for 32 times in the wavenumber range of 400 cm^{-1} to 4000 cm^{-1}. The FTIR spectra of AO-60/NBR composites were acquired from sheet specimens with a thickness of approximately 1 mm by using the attenuated total reflection (ATR) technique. DSC measurements were performed on a TGA/DSC calorimeter made by Mettler-Toledo Co (Switzerland). Samples weighing about 10 mg and sealed in aluminum were heated from -60℃ to 150℃ at a heating rate of 10 ℃/min under a nitrogen atmosphere. The glass transition temperature (*Tg*) was identified by the midpoint of the transition region. Dynamic mechanical measurements were carried out in the tension mode by using a VA 3000 dynamic mechanical analyzer (DMA) made by Rheometric Scientific Inc. (USA). The rectangular samples were 12 mm long, 6 mm wide, and about 2 mm thick. The temperature dependence of the loss factor (tan δ) for various samples was measured between -50℃ and 100℃ at a constant frequency of 1 Hz and a heating rate of 5℃/min.

3.4 Microscopic morphology analysis

RSC Advances Accepted Manuscript

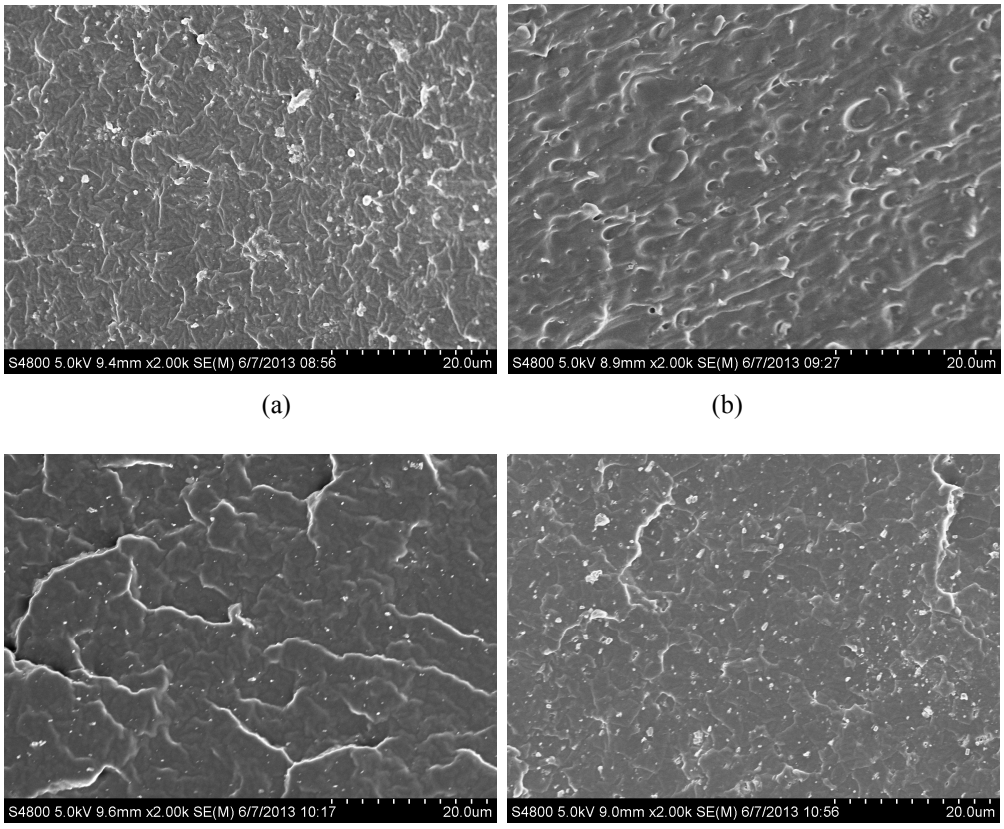

Fig. 7 SEM images of (a) N220S, (b) AO-60/N220S (73/100), (c) N230S, and (d) AO-60/N230S (73/100).

Fig. 7 shows the microscopic images of the representative fracture surfaces of AO-60/NBR composites at the same magnification. The fracture surfaces of AO-60/NBR composites are homogeneous in pure NBR and at an AO-60 content of 36 phr, because most AO-60 molecules are dissolved to form a fine dispersion in the matrix. As the AO-60 content exceeds 36 phr, AO-60 has a poor dispersion and phase separates in the N220S matrix, as indicated by the numerous holes resulting from the removal of AO-60 molecules from the fracture surface in Fig. 7 (b). However, Fig. 7 (d) shows that the fracture surface of the AO-60/N230S composite is very smooth and without any holes, probably because of the good compatibility and strong interactions

RSC Advances Accepted Manuscript

between AO-60 and the N230S matrix.[40] These results are consistent with the MD simulation results above and are further supported by the DSC and DMA results below.

3.5 FTIR analysis of hydrogen bonds in AO-60/NBR composites

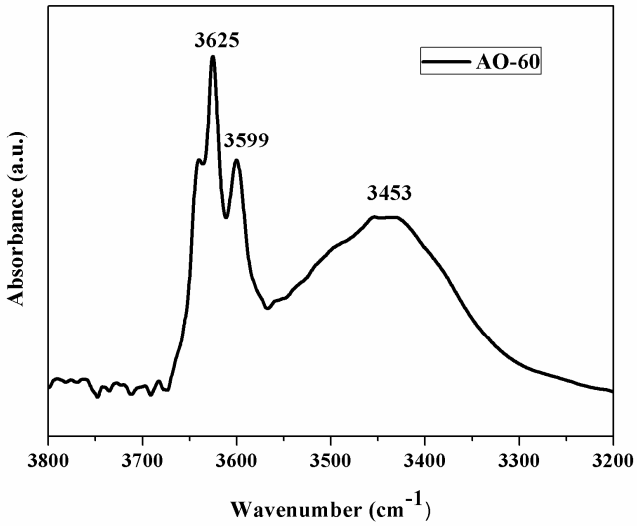

(a)

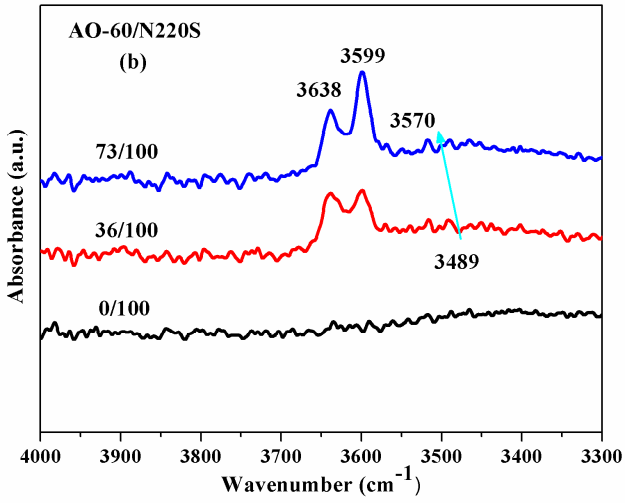

(b)

RSC Advances Accepted Manuscript

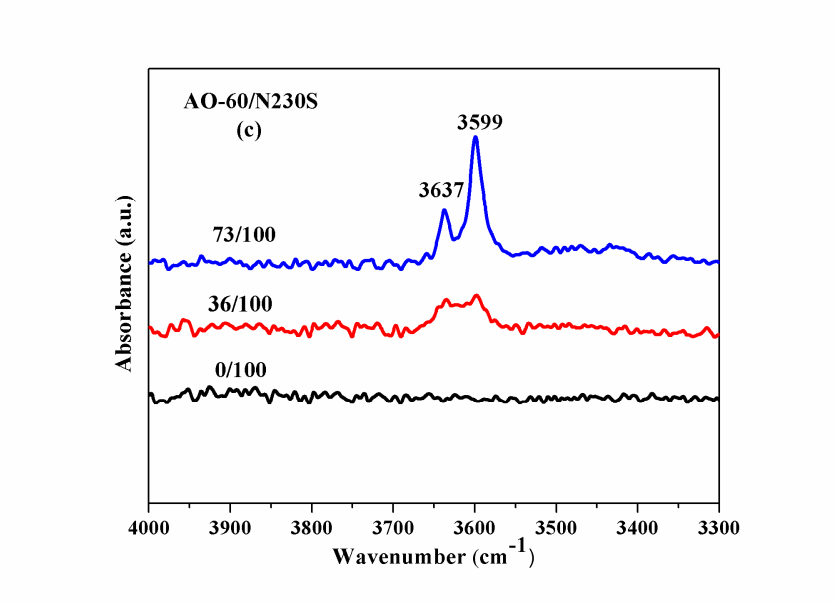

(c)

Fig. 8 FTIR/TR spectrum of (a) AO-60, (b) FTIR/ATR spectra of AO-60/N220S composites., and (c) FTIR/ATR spectra of AO-60/N230S composites.

To examine the intermolecular interaction between N220S (or N230S) and AO-60, we obtained FTIR measurements of pure N220S, pure N230S, AO-60/N220S composite, and AO-60/N230S composite were obtained. In Fig. 8 (a) for AO-60, there are the significant absorptions in 3550-3675 cm^{-1} and 3350-3550 cm^{-1}, which are assigned to the -OH vibrations caused by free -OH and the OH-OH interactions (O-H···O hydrogen bonds) between AO-60 molecules, respectively.[35] The spectra of the pure N220S and N230S hardly reveal any absorbance band in the wavenumber range 3200-4000 cm^{-1} in Fig.8 (b) and Fig.8 (c), whereas the spectra of the AO-60/N220S and AO-60/N230S composites indicate significant peaks at 3638 cm^{-1} and 3599 cm^{-1}, corresponding to the free -OH of AO-60. Moreover, a broad peak appears in the range 3350-3550 cm^{-1}, which can be attributed to the hydrogen bonding between the -OH groups of AO-60 and the -CN groups of NBR.

3.6 Verification of compatibility by DSC analysis

RSC Advances Accepted Manuscript

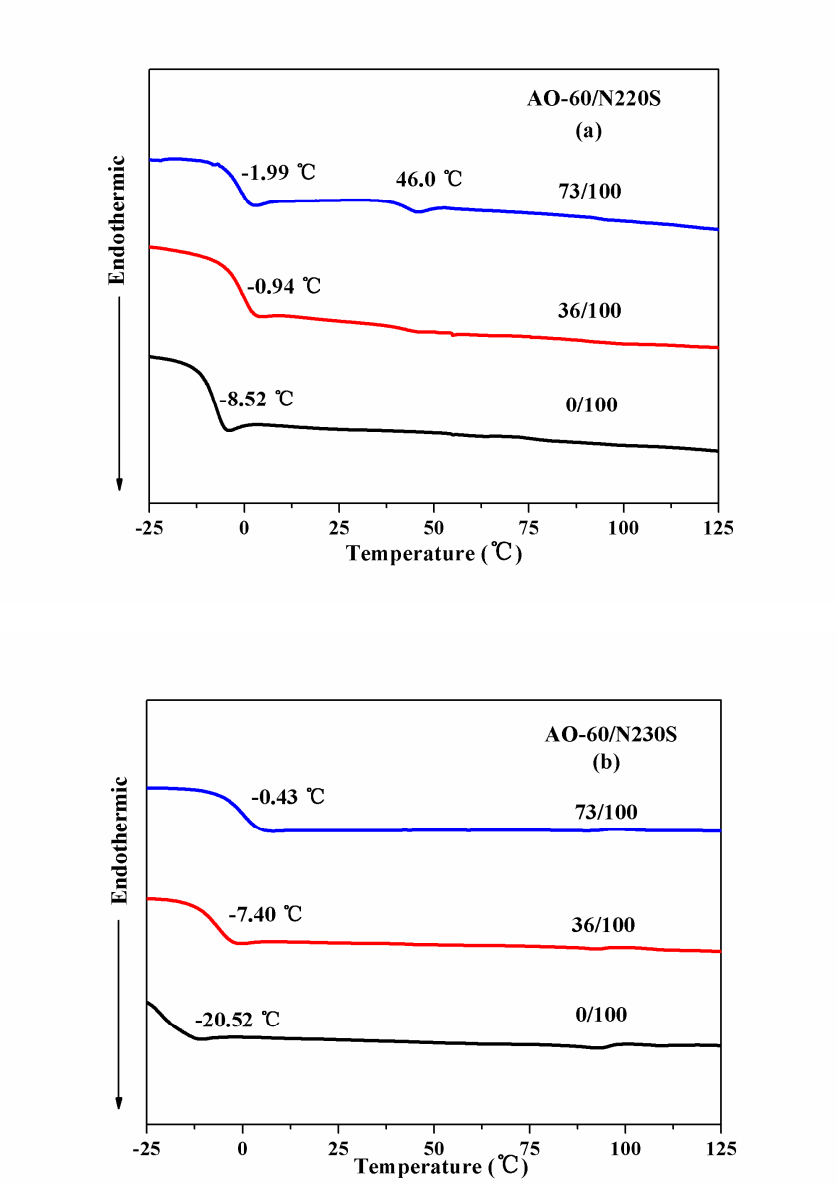

Fig. 9 DSC thermograms: (a) AO-60/N220S composite and (b) AO-60/N230S composite.

The occurrence of glass transition can be used as a rule of thumb to determine the compatibility of blend. If a binary blend is compatibility, only a single glass transition appears. [41] Otherwise, two glass transitions could be detected and each glass transition indicates the freezing temperature of one component.[42] Fig. 9 shows the DSC thermograms of the AO-60/N220S composite and the AO-60/N230S composite.

RSC Advances Accepted Manuscript

As can be seen from Fig. 9 (a) and (b), the *Tg* of NBR increases with the increase of acrylonitrile content because the side chains and polarity of NBR increase with the increase of acrylonitrile content, making macromolecular chain movements difficult.

The *Tg* of an AO-60/NBR composite is significantly higher than that of the pure NBR because the small AO-60 molecules have strong molecular interaction with the NBR matrix. Moreover, the AO-60/N230S composite shows only one *Tg*, indicating the good compatibility between AO-60 and the N230S matrix. However, there are two *Tgs* in the AO-60/N220S composite when the content of AO-60 is above 36 phr, indicating poor compatibility and a two-phase structure. The temperature of 46℃ indicated in the DSC curve is the glass transition temperature of the amorphous AO-60 that has aggregated in the matrix.[43]

3.7 Dynamic mechanical properties

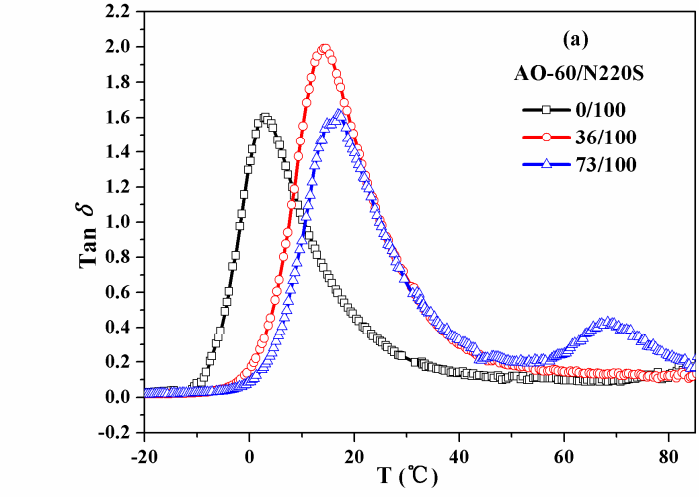

RSC Advances Accepted Manuscript

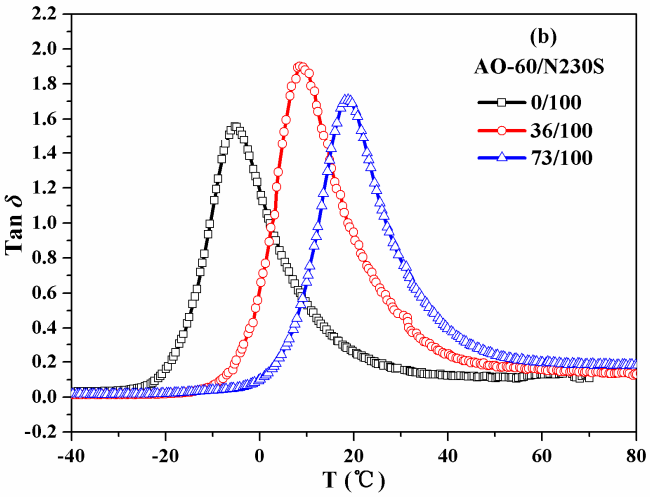

Fig. 10 Temperature dependence of loss tangent (tan δ): (a) AO-60/N220S composite and (c) AO-60/N230S composite.

Fig. 10 shows the temperature dependence of the loss tangent (tan δ) for the AO-60/N220S composite and the AO-60/N230S composite. It can be seen that pure N220S and N230S show only one tan δ peak. In addition, the tan δ peak increases and gradually shifts to higher temperatures with increasing acrylonitrile content. The shift was mainly due to the increase in polarity with increasing acrylonitrile content, resulting in the increase in friction between molecular chains and high energy consumption. As the AO-60 content exceeds 36 phr, two tan δ peaks appear in the AO-60/N220S composite, an indication of phase separation. The DSC results presented above indicated that the excessive AO-60 small molecules aggregated, leading to the appearance of two phases in the composite. However, there is only one tan δ peak in the AO-60/N230S composite, indicating the good compatibility between N230S and AO-60.

Table 5 shows the damping properties of N220S, N230S, the AO-60/N220S

RSC Advances Accepted Manuscript

composite, and the AO-60/N230S composite. The area under the tan δ versus temperature curve (TA) is commonly used for characterizing the damping property of rubber.[44] The larger the TA value, the better the damping properties of material. Table 5 shows that AO-60/N230S has the larger TA value and wider temperature range over which the damping is efficient (tan δ > 0.3) at the same AO-60 content, indicating better damping properties, confirming the MD simulation results.

Table 5 Damping properties of N220S, N230S, the AO-60/N220S composite, and the AO-60/N230S composite

Materials	Mass ratios	Tan δ_{max}		tan δ > 0.3	
		Value	T (℃)	ΔT	TA (℃)
AO-60/N220S	0/100	1.60	3.10	31.3	40.7
	36/100	2.00	14.6	39.0	55.9
	73/100	1.62	16.9	36.4	49.1
AO-60/N230S	0/100	1.55	-5.25	33.8	39.4
	36/100	1.95	8.5	39.2	56.5
	73/100	1.71	18.8	37.8	53.7

4 Conclusions

MD simulation and experiments have been adopted to analyze the compatibility, microstructure, and damping properties of AO-60/NBR composites with different acrylonitrile contents. The solubility parameter δ, number of H-bonds, and binding energy of the AO-60/NBR composites are calculated by MD simulation. N230S with an acrylonitrile content of 34% has a good compatibility with AO-60, but N220S with an acrylonitrile content of 41% has a poor compatibility with AO-60, as predicated by MD simulation. AO-60/N230S has larger H-bonds and higher binding energy than AO-60/N220S both indicating the stronger interactions between AO-60 and N230S

RSC Advances Accepted Manuscript

and better damping performance of AO-60/N230S. Both predictions are confirmed by SEM, DSC, and DMA analyses. The combined simulation and experimental study provides a theoretical understanding of the effect of acrylonitrile content in NBR on the compatibility and damping properties of AO-60/NBR composites on a molecular level.

Acknowledgments

The financial supports of the National Natural Science Foundation of China under Grant No. 51473012 are gratefully acknowledged.

Notes and references

Beijing Engineering Research Center of Advanced Elastomers, Beijing University of Chemical Technology, Beijing 100029, P.R. China
Fax: 86-10-64433964; E-mail: wusz@mail.buct.edu.cn

1 A. A. Gusev, K. Feldman and O. Guseva, *Macromolecules*, 2010, **43**, 2638-2641.

2 Y. Q.Wang, Y.Wang, H. F. Zhang and L. Q Zhang, *Macromol Rapid Commun*, 2006**,** **27**, 1162-1167.

3 S. Joseph, P. A. Sreekumar, J. M. Kenny, D. Puglia, S. Thomas and K. Joseph, *Polym Compos*, 2010, **31**, 236-244.

4 X. Y. Zhao, Y. L. Lu, D. L. Xiao, S. Z. Wu and L. Q. Zhang, *Macromol Mater Eng*, 2009, **294**, 345-351.

5 C. Wu, T. A. Yamagishi, Y. Nakamoto, S. I. Ishida, K. H. Nitta and S. Kubota, *J Polym Sci, Part B: Polym Phys*, 2000, **38**, 1341-1347.

RSC Advances Accepted Manuscript

6 C.Wu, T. A. Yamagishi, Y. Nakamoto, S. Ishida, K. H. Nitta and S. Kubota, *J Polym Sci, Part B: Polym Phys*, 2000, **38**, 2285-2295.

7 Q. Liu, H. Zhang and X. Yan, *Iran Polym J*, 2009, **18**, 401-413.

8 T. Sajjayanukul, P. Saeoui and C. Sirisinha, *J Appl Polym Sci*, 2005, **97**, 2197-2203.

9 A. Omayu, T. Ueno and A. Matsumoto, *Macromol Chem Phys*, 2008**, 209**, 1503-1514.

10 C. Wu, Y. Otani, N. Namiki, H. Emi, K. H. Nitta and S. Kubota, *J Appl Polym Sci*, 2001, **82**, 1788-1793

11 X. Y. Zhao, P. Xiang, M. Tian, H. Fong, R. Jin and L. Q. Zhang, *Polymer*, 2007, **48**, 6056-6063.

12 P. Xiang, X. Y. Zhao, D. L. Xiao, Y. L. Lu and L. Q. Zhang, *J Appl Polym Sci*, 2008**, 109**, 106-114.

13 M. Song, X. Y. Zhao, Y. Li, S. K. Hu, L. Q. Zhang and S. Z. Wu, *RSC Adv***,** 2014, **4**, 6719-6729.

14 J. H. Zhang, L. F. Wang and Y. F. Zhao, *Mater Design*, 2013, **51**, 648-657.

15 X. Y. Zhao, Y. J. Cao, H. Zou, J. Li and L. Q. Zhang, *J Appl Polym Sci*, 2011, **123**, 3696-3702.

16 J. E. Mark, *Rubberlike Elasticity*, *2nd ed*., Wiley-Intersecience: New York, 2007.

17 X. Y. Zhao, Y. L. Lu, D. L. Xiao, S. Z. Wu and L. Q. Zhang, *Macromol Mater Eng*, 2009, **294**, 345-351.

18 B. Likozar and Z. Major, *Appl Surf Sci*, 2010, **257**, 565-573.

19 T. Yasin, S. Ahmed, F. Yoshii and K.Makuuchi, *React Funct Polym*, 2003, **57**,

RSC Advances Accepted Manuscript

113-118.

20 M. E. Lauer, O. Grassmann, M. Siam, J. Tardio, L. Jacob, S. Page, J. H. Kindt, A. Engel and J. Alsenz, *Pharm Res*, 2011, **28**, 572-584.

21 C. Dyer, Z. Jiang, J. Bozell, T. Rials, W. T. Heller and M. Dadmun, *Soft Matter*, 2013, **9**, 3402-3411.

22 X. J. Li, S. L. Zhang, H. Wang, C. F. Zhang, J. H. Pang, J. X. Mu, G. Ma, G. B. Wang and Z. H. Jiang, *Polym Int*, 2011, **60**, 607-612.

23 S. Ramanaiah, P. R. Rani, T. V. M. Sreekanth and K. S. Reddy, *J Macromol Sci B*, 2011, **50**, 551-562.

24 K. Lewandowska, *Thermochim Acta*, 2011, **517**, 90-97.

25 Z. L. Luo and J. W. Jiang, *Polymer*, 2010, **51**, 291-299.

26Y. Y. Gao, J. Liu, D. P. Cao and L. Q. Zhang, *RSC Adv***,** 2013, **3**, 21655-21665.

27 Q. Yang, X. P. Yang, X. D. Li, L. Shi and G. Sui, *RSC Adv***,** 2013, **3**, 7452-7459.

28 S. W. Bunte and H. Sun, *J Phys Chem B*, 2000, **104**, 2477-2489.

29 S. Zhu, L. Yan, D. Zhang and Q. Feng, *Polymer*, 2011, **52**, 881-892.

30 J. Colmenero, F. Alvarez and A. Arbe, *Phys Rev E*, 2002, **65**, 1804-1815.

31 J. E. Basconi and M. R.Shirts, *J Chem Theory Comput*, 2013, **9**, 2887-2899.

32 J. Davoodi and M. Ahmadi, *Compos Part B-Eng*, 2012, **43**, 10-14.

33 X. F. Ma, W. H. Zhu, J. J. Xiao, H. M. Xiao, *J Hazard Mater*, 2008, **156**, 201-207.

34 L. Qiu and H. M. Xiao, *J Hazard Mater*, 2009, **164**, 329-336.

35 B. Qiao, X. Y. Zhao, D. M. Yue, L. Q. Zhang and S. Z. Wu, *J Mater Chem*, 2012, **22**, 12339-12348.

RSC Advances Accepted Manuscript

36 X. J. Wang, J. J. Xiao, W. H. Zhu, H. Sun and H. M. Xiao, *J Hazard Mater*, 2009, **167**, 810-816.

37 J. Gupta, C. Nunes, S. Vyas and S. Jonnalagadda, *J. Phys. Chem. B*, 2011, **115**, 2014-2023.

38 A. Forster, J. Hempenstall, I. Tucker and T. Rades, *Int. J Pharm Sci*, 2001, **226**, 147-161.

39 D. J. Greenhalgh, A. C. Williams, P. Timmins and P. York, *J Pharm Sci*, 1999, **88**, 1182-1190.

40 H. Li, J. Q. Zhao, S. M. Liu and Y. C. Yuan, *RSC Adv***,** 2014, **4**, 10395-10401.

41 H. Yang, Z. S. Li, Z. Y. Lu and C. C. Sun, *Eur Polym J*, 2005, **41**, 2956-2962.

42 H. Yang, L. Z. Sheng, H. J. Qian, Y. B. Yang, X. B. Zhang and C. C. Sun, *Polymer*, 2004, **45**, 453-457.

43 X. Y. Zhao, P. Xiang and L. Q. Zhang, *Acta Mater Compos Sinica*, 2007, **24**, 44-49.

44 Z. Gu, X. Zhang, C. Bao, F. Fang, X. Ding, S. Y. Li, L. Chen, M. Xue, H. Wang and X. Y. Tian, *J Non-Cryst Solids*, 2014, **388**, 17-22.

RSC Advances Accepted Manuscript

Graphical Abstract

Title: Effect of acrylonitrile content on compatibility and damping properties of hindered phenol AO-60/nitrile-butadiene rubber composites: Molecular dynamics simulation

Authors: Meng Song, Xiuying Zhao, Yi Li, Tung W. Chan , Liqun Zhang and Sizhu Wu *

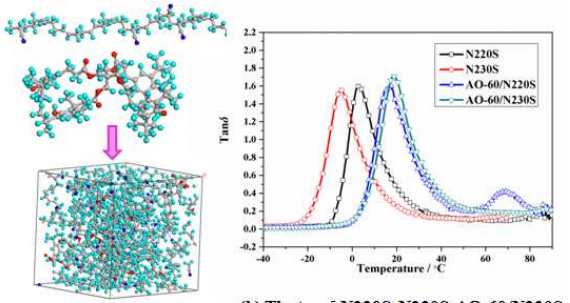

(a) MD simulation of AO-60/NBR

(b) The tan δ N220S, N230S, AO-60/N220S composite, and AO-60/NBR composite

By combining molecular dynamics simulations and experiment, the effect of acrylonitrile content on compatibility and damping properties were investigated in the AO-60/ nitrile-butadiene rubber composites.

RSC Advances Accepted Manuscript